Lecture Notes in Electrical Engineering 1164

Serge Pierfederici
Jean-Philippe Martin *Editors*

ELECTRIMACS 2022

Selected Papers – Volume 2

Springer

Lecture Notes in Electrical Engineering

Volume 1164

The book series *Lecture Notes in Electrical Engineering* (LNEE) publishes the latest developments in Electrical Engineering—quickly, informally and in high quality. While original research reported in proceedings and monographs has traditionally formed the core of LNEE, we also encourage authors to submit books devoted to supporting student education and professional training in the various fields and applications areas of electrical engineering. The series cover classical and emerging topics concerning:

- Communication Engineering, Information Theory and Networks
- Electronics Engineering and Microelectronics
- Signal, Image and Speech Processing
- Wireless and Mobile Communication
- Circuits and Systems
- Energy Systems, Power Electronics and Electrical Machines
- Electro-optical Engineering
- Instrumentation Engineering
- Avionics Engineering
- Control Systems
- Internet-of-Things and Cybersecurity
- Biomedical Devices, MEMS and NEMS

For general information about this book series, comments or suggestions, please contact leontina.dicecco@springer.com.
To submit a proposal or request further information, please contact the Publishing Editor in your country:

China

Jasmine Dou, Editor (jasmine.dou@springer.com)

India, Japan, Rest of Asia

Swati Meherishi, Editorial Director (Swati.Meherishi@springer.com)

Southeast Asia, Australia, New Zealand

Ramesh Nath Premnath, Editor (ramesh.premnath@springernature.com)

USA, Canada

Michael Luby, Senior Editor (michael.luby@springer.com)

All other Countries

Leontina Di Cecco, Senior Editor (leontina.dicecco@springer.com)

**** This series is indexed by EI Compendex and Scopus databases. ****

Serge Pierfederici • Jean-Philippe Martin
Editors

ELECTRIMACS 2022

Selected Papers – Volume 2

Springer

Editors
Serge Pierfederici
Université de Lorraine, CNRS, LEMTA
Nancy, France

Jean-Philippe Martin
Université de Lorraine, CNRS, LEMTA
Nancy, France

ISSN 1876-1100 ISSN 1876-1119 (electronic)
Lecture Notes in Electrical Engineering
ISBN 978-3-031-55695-1 ISBN 978-3-031-55696-8 (eBook)
https://doi.org/10.1007/978-3-031-55696-8

This Springer imprint is published by the registered company Springer Nature Switzerland AG
The registered company address is: Gewerbestrasse 11, 6330 Cham, Switzerland

Preface to Electrimacs 2022, Volume 2

ELECTRIMACS is the short and well-known name of the international conference of the IMACS TC1 Committee. The conference is focused on the theory and application of modelling, simulation, analysis, design, optimization, identification and diagnostics in electrical power engineering. The conference is a meeting point for researchers to share ideas and advances in the broad fields of electric machines and electromagnetic devices, power electronics, transportation systems, smart grids, electric and hybrid vehicles, renewable energy systems, energy storage, batteries, supercapacitors and fuel cells.

ELECTRIMACS 2022 was held in Nancy, France, from 16 to 19 May 2022. Three tutorial sessions, 20 oral sessions, 4 technical tracks, 4 plenary sessions with thought leaders from academia and research centers, and six special sessions were included in the conference program. The conference hosted 102 oral presentations of papers, selected among 120 submissions received. The review process involved at least three reviewers per paper.

The main institutional sponsor of the conference is the Université de Lorraine. The conference also received technical co-sponsorship from the important scientific society IMACS, and a financial co-sponsorship from Region Lorraine. Private companies sponsored the event or took part in the industrial exhibit.

This book collects a selection of 21 papers presented at ELECTRIMACS 2022 Nancy. These papers are particularly focused on modelling and computational simulations applied to energy systems and smart grids.

The collection is organized into two thematic parts: Modelling and Computational Simulation for Energy Systems, and Modelling and Computational Simulation for Control and Optimization in Electrical Power Systems and Smart Grids.

General Chairs

Jean-Philippe Martin, Université de Lorraine, France
Serge Pierfederici, Université de Lorraine, France

Local Organising Committee
Thierry Boileau, UL, France
Farid Meibody-Tabar, UL, France
Babak Nahid-Mobarakeh, McMaster University, Canada
Ignace Rasoanarivo, UL, France
Noureddine Takorabet, UL, France
Matthieu Urbain, UL, France
Mathieu Weber, CNRS, France

Technical Program Chairs
Ramon Blasco-Gimenez, Universitat Politécnica de Valéncia, Spain
Eric Monmasson, Université de Cergy-Pontoise, France
Benoit Robyns, HEI Lille, France
Giovanni Spagnuolo, Università degli studi di Salerno, Italy

Track Chairs
Seiichiro Katsura, Keio University, Dept. of System Design Engineering, Yokohama, Japan
Nicolas Patin, UTC Compiègne, LEC, Compiègne, France
Georges Barakat, Université Le Havre Normandie, GREAH, Le Havre, France
Noureddine Takorabet, Université de Lorraine, GREEN, Nancy, France
João Pedro Trovão, University of Sherbrooke, e-TESC Lab, Sherbrooke, Canada
Bruno Francois, Ecole Centrale de Lille, L2EP, Lille, France
Manuela Sechilariu, UTC Compiègne, AVENUES, Compiègne, France
Bruno Sareni, Université Paul Sabatier, ENSEEIHT, Toulouse, France
Maria Carmela di Piazza, CNR, Palermo, Italia
Afef Bennani Ben Abdelghani, University of Carthage, INSAT, Tunis, Tunisia
Frédéric Richardeau, CNRS Dir., LAPLACE, University of Toulouse, CNRS, UPS, Toulouse, France
Rodolfo Araneo, Dipartimento di Ing. Astronautica, Elettrica ed Energetica, Sapienza Università di Roma, Italy
Giuseppe La Tona, Institute of Marine Engineering of National Research Council (CNR), Italy
Giovanni Petrone, DIEM - Dipartimento di Ingegneria dell'Informazione ed Elettrica e Matematica Applicata, Università degli studi di Salerno, Italy
Massimiliano Luna, Institute of Marine Engineering of National Research Council (CNR), Italy
Walter Zamboni, DIEM - Dipartimento di Ingegneria dell'Informazione ed Elettrica e Matematica Applicata, Università degli studi di Salerno, Italy
Salvy Bourguet, Université de Nantes, IREENA, France
Benoit Delinchant, Université Grenoble Alpes, G2Elab, France
Samir Jemei, Univ. Bourgogne Franche-Comté, FEMTO-ST Institute, FCLAB, CNRS, Belfort, France
Mohsen Kandidayeni, University of Sherbrooke (e-TESC lab) and University of Quebec in Trois-Rivières (IRH lab), Quebec, Canada

François Vallee, University of Mons, Power Systems & Markets Research Group, Mons, Belgium
Vincent Debusschere, Université Grenoble Alpes, G2ELAB - ENSE3 Grenoble INP, France

Scientific Committee

Ennio Andrea Adinolfi	Italy
Giovanni Lutzemberger	Italy
Ennio Andrea Adinolfi	Italy
Giovanni Lutzemberger	Italy
Giovanna Adinolfi	Italy
Jean Mahseredjian	Canada
Yacine Amara	France
Mariusz Malinowski	Poland
Julia Amici	Italy
Patrizio Manganiello	Netherlands
Giovanni Battista Appetecchi	Italy
Emmanuel Marcault	France
Seddik Bacha	France
Fabrizio Marignetti	Italy
Lotfi Baghli	France
Jean-Philippe Martin	France
Mahmoud Barakat	France
Nicolas Mary	Canada
Georges Barakat	France
Hajer Marzougui	Tunisia
Efstratios Batzelis	United Kingdom
Alessandro Massi Pavan	Italy
Hector Beltran	Spain
Paolo Mattavelli	Italy
Afef Ben Abdelghani-Bennan	Tunisia
Pascal Maussion	France
Manel Ben Ghorbal	Tunisia
Farid Meibody-Tabar	France
Mohamed Benbouzid	France
Alexander Micallef	Malta
Mohamed Fouad Benkhoris	France
El Hadj Miliani	France
Michel Benne	France
Marta Molinas	Norway
Olivier Bethoux	France
Nazih Moubayed	Lebanon

Nicu Bizon	Romania
Piercarlo Mustarelli	Italy
Frede Blaabjerg	Denmark
Babak Nahidmobarakeh	Canada
Silvia Bodoardo	Italy
Wissem Naouar	Tunisia
Thierry Boileau	France
Maria Assunta Navarra	Italy
Loic Boulon	Canada
Radouane Ouladsine	Morocco
Salvy Bourguet	France
Djaffar Ould Abdeslam	France
Alain Bouscayrol	France
Yoann Pascal	France
Gianluca Brando	Italy
Nicolas Patin	France
Giovanni Brunaccini	Italy
Alireza Payman	France
Piergiacomo Cancelliere	Italy
Marie-Cecile Pera	France
Jean-Frederic Charpentier	France
Emilio Pérez Soler	Spain
Daniele Davino	Italy
Giovanni Petrone	Italy
Alexandre De Bernardinis	France
Matheepot Phattanasak	Thailand
Bruno Dehez	Belgium
Maria Pietrzak-David	France
Louis-A. Dessaint	Canada
Pierpaolo Polverino	Italy
Luigi Di Benedetto	Italy
Arturo Popoli	Italy
Maria Carmela Di Piazza	Italy
Miguel Pretelli	Italy
Christian Dufour	Canada
Ionela Prodan	France
Benoit Durillon	France
Mohammad Rafiei	Italy
Maurice Fadel	France
Bertrand Raison	France
Erina Ferro	Italy
Hubert Razik	France
Bruno Francois	France

Mattia Ricco	Italy
Fei Gao	France
Javier Riedemann	Chile
Luis Antonio Garcia Gutierrez	France
Delphine Riu	France
Jean-Paul Gaubert	France
Xavier Roboam	France
Jean-Yves Gauthier	France
Robin Roche	France
Roghayeh Gavagsaz	Iran
António Roque	Portugal
Joern Geisbuesch	Germany
Paola Russo	Italy
Chris Gerada	United Kingdom
Sébastien Sanchez	France
Malek Ghanes	France
Francisco José Sánchez Pacheco	Spain
Francesco Grasso	Italy
Bruno Sareni	France
Francesco Grimaccia	Italy
Christophe Saudemont	France
Giambattista Gruosso	Italy
Manuela Sechilariu	France
Josep Guerrero	Denmark
Samuel Simon Araya	Denmark
Pierluigi Guerriero	Italy
Jacopo Sini	Italy
Ruben Sigifredo Pena Guinez	Chile
Sondes Skander Mustapha	Tunisia
Alonso Gutierrez Galeano	France
Ilhem Slama-Belkhodja	Tunisia
Mickael Hilairet	France
Francesca Soavi	Italy
Samir Hlioui	France
Cyril Spiteri Staines	Malta
Azeddine Houari	France
Kateryna Stoyka	Italy
Diego Iannuzzi	Italy
Phatiphat Thounthong	Thailand
Nadir Idir	France
Francesco Antonio Tiano	Italy
Lahoucine Id-Khajine	France
Abdelmounaim Tounzi	France

Samir Jemei	France
Joao Pedro Trovao	Canada
Wattana Kaewmanee	Thailand
Andrea Trovò	Italy
Hadi Kanaan	Lebanon
Christophe Turpin	France
Seiichiro Katsura	Japan
Seppo Valkealahti	Finland
Youssef Kraiem	France
Philippe Viarouge	Canada
Alexander Kuznietsov	Germany
Dmitri Vinnikov	Estonia
Patrizia Lamberti	Italy
Stephane Vivier	France
Kari Lappalainen	Finland
Hanqing Wang	France
Antonino Laudani	Italy
Xin Wen	France
Walter Lhomme	France
Lin-Shi Xuefang	France
Elizaveta Liivik	Estonia
Medhi Zadeh	Norway
Marco Liserre	Germany
Walter Zamboni	Italy
Ramon Lopez Erauskin	Spain
Majid Zandi	Iran
Massimiliano Luna	Italy
Rongwu Zhu	Germany
Blake Lundstrom	United States
Hesan Ziar	Netherlands

Nancy, France

Serge Pierfederici
Jean-Philippe Martin

Contents

Part I Modelling and Computational Simulation for Energy Systems

1 Efficiency Maps of Synchronous Machines Based on Electrical Circuits Modelling 3
Haidar Diab, Salim Asfirane, Yacine Amara, Hamid Ben Ahmed, and Mohamed Gabsi

2 Losses Prediction in the Frequency Domain for Voltage Source Inverters 23
Hugot Pichon, Yves Lembeye, and Jean-Christophe Crebier

3 Online Detection of PV Degradation Effects Through ANN Classifier 37
Rudy Alexis Guejia Burbano, Vincenzo Noviello, and Giovanni Petrone

4 Modeling the Non-linearities of Charge-Transfers and Solid Electrolyte Interphase Resistances for a Sodium-Ion Battery with a Hard Carbon Electrode 53
Houssam Rabab, Nicolas Damay, Fernanda Vendrame, Christophe Forgez, and Asmae El Mejdoubi

5 Experimental Development of Embedded Online Impedance Spectroscopy of Lithium-Ion Batteries – Proof of Concept and Validation 67
Sudnya Vaidya, Daniel Depernet, Daniela Chrenko, and Salah Laghrouche

6 An Improved Maximum Power Point Tracking for Photovoltaic Distributed Energy System Associated with a Shunt Active Power Filter 85
Rosalie Rouphael, Ahmad Ghamrawi, Nezha Maamri, and Jean-Paul Gaubert

7 Modeling Battery Aging Through High-Current Incremental Capacity Features in Fast Charge Cycling 101
Ludovico Lombardi, Eric Monmasson, Brian Ospina Agudelo, and Walter Zamboni

8 Fully Decentralized Control Strategy for Synchronous Open-Winding Motors 115
Louis Dassonville, Jean-Yves Gauthier, Xuefang Lin-Shi, and Ali Makki

9 Quasi 3D Reluctance Network Modeling of an Axial Flux Switched Reluctance Machine 129
Mostafa Hatoum, Salim Asfirane, Georges Barakat, and Yacine Amara

10 A Voltage-Controlled Split-pi Converter Interfacing a High-Voltage ESS with a DC Microgrid: Modeling and Experimental Validation 145
Massimiliano Luna, Antonino Sferlazza, Angelo Accetta, Maria Carmela Di Piazza, Giuseppe La Tona, and Marcello Pucci

11 Co-Simulation Domain Decomposition Algorithm for Hybrid EMT-Dynamic Phasor Modeling 163
Hélèna Shourick, Damien Tromeur-Dervout, and Laurent Chédot

Part II Modelling and Computational Simulation for Control and Optimisation in Electrical Power Systems and Smart Grids

12 Uncertainties Impact and Mitigation with an Adaptive Model-Based Voltage Controller 179
Muhammad Andy Putratama, Rémy Rigo-Mariani, Vincent Debusschere, and Yvon Bésanger

13 Consensus-Based Distributed Primary Control for Accurate Power Sharing in Islanded Mesh Microgrids 199
Youssef Hennane, Abdelmajid Berdai, Jean-Philippe Martin, Serge Pierfederici, and Farid Meibody-Tabar

14 Model-Free Detection of Distributed Solar Generation in Distribution Grids Based on Minimal Exogenous Information 213
Aleksandr Petrusev, Rémy Rigo-Mariani, Vincent Debusschere, Patrick Reignier, and Nouredine Hadjsaid

15 A Q-Learning-Based Energy Management Strategy for a Three-Wheel Multi-Stack Fuel Cell Hybrid Electric Vehicle 233
Razieh Ghaderi, Mohsen Kandidayeni, Loïc Boulon, and João P. Trovão

16 Load Consumption Characterization and Tariff Design Based on Data Mining Techniques 243
Sérgio Ramos, Hugo Morais, João Soares, Zahra Foroozandeh, and Zita Vale

17 Energy Management System by Deep Reinforcement Learning Approach in a Building Microgrid 257
Mohsen Dini and Florence Ossart

18 Passivity Based Control of Two Distributed Generations in DC Microgrid 271
Roghayeh Gavagsaz-Ghoachani, Matheepot Phattanasak, Jean-Philippe Martin, and Serge Pierfederici

19 An Improved Control of High Efficiency Series Converter for Fuel Cell/Supercapacitor Hybrid System 283
A. Siangsanoh, W. Kaewmanee, R. Gavagsaz-Ghoachani, J. P. Martin, M. Weber, M. Phattanasak, S. Pierfederici, G. Maranzana, and S. Didierjean

20 Photovoltaics at the Electric Mobility's Service: French Case Study 297
Khaled Hajar, Reza Razi, Majid Mehrasa, Antoine Labonne, Ahmad Hably, and Seddik Bacha

21 Enhanced Performances of the DFIG Power Control Using the Exponential Reaching Law Based Sliding Mode Control 311
Dekali Zouheyr, Baghli Lotfi, and Boumediene Abdelmadjid

Part I
Modelling and Computational Simulation for Energy Systems

Chapter 1
Efficiency Maps of Synchronous Machines Based on Electrical Circuits Modelling

Haidar Diab, Salim Asfirane, Yacine Amara, Hamid Ben Ahmed, and Mohamed Gabsi

Abstract In many electrical machines applications, as electrical vehicles, the operating conditions are largely varying. Efficiency maps constitute then a convenient way to assess motor designs and their control strategies. This contribution presents the development of a software tool allowing the computation of efficiency maps of synchronous machines. This tool could be applied to all synchronous machines types: wound field, PM, hybrid excited and synchronous reluctance motors.

1.1 Introduction

This contribution presents the detailed development of a software tool used to compute the efficiency maps (EM) of all synchronous motors types: wound field, PM, hybrid excited and synchronous reluctance motors. Efficiency maps constitute a convenient way to assess motor designs and their control strategies [1–18].

The electric traction is chosen as the case study. For this application, the traction motor is often operating in partial load regions, which requires optimising the power efficiency in these regions in order to achieve high energy efficiency. The developed tool can be used for that purpose, through the analysis of the effect of the synchronous machines parameters on the EM [17].

Previous works done on non-salient synchronous machines [16, 17], which excludes synchronous reluctance motors, are used as a reference to assess the validity of this new developed tool. Works done on maximum power capability of

H. Diab · S. Asfirane · Y. Amara (✉)
GREAH, Université Le Havre Normandie, Le Havre, France
e-mail: yacine.amara@univ-lehavre.fr

H. B. Ahmed
SATIE, UMR CNRS 8029, École normale supérieure de Rennes, Bruz, France

M. Gabsi
SATIE, UMR CNRS 8029, École Normale Supérieure Paris-Saclay, Cachan, France

S. Pierfederici, J.-P. Martin (eds.), *ELECTRIMACS 2022*, Lecture Notes in Electrical Engineering 1164, https://doi.org/10.1007/978-3-031-55696-8_1

synchronous machines will also be used for that purpose. This tool will be made available to the readers.

If following sections, an overview of the use of EM for performance assessment and as a predesign tool is first presented in Sect. 1.2. Then, the electrical circuits modelling approach adopted to study the different synchronous machines types is presented in Sect. 1.3. The versatility of adopted approach is highlighted. The use of normalized parameters is also discussed as a mean of drawing general conclusions. The EM computation, based on the adopted modelling approach, is then detailed in Sect. 1.4 for salient poles machines. The main novelty of this contribution, as compared to previously published contributions [4, 6, 15–17], is the consideration of saliency. Section 1.5 is dedicated to the validation of developed tool. Results obtained from the newly developed tool are compared to previously published works, for that purpose. Finally, the tool is exploited to highlight the effect of saliency ratio on the synchronous machines EM, and some conclusions and perspectives are presented.

1.2 Efficiency Maps (EM) as a Predesign Tool

Efficiency mapping for electrical machines, with a wide operating range, which is typically the case for electric vehicles, can be used whether for performance assessment of constructed machines [2, 19], or upstream as a powerful conception and design tool to improve their energy efficiency [1–18]. Increasing the energy efficiency of electrical vehicles powertrains helps reduce their energy consumption, and improve their autonomy [20].

Efficiency mapping, whether in (Torque, Speed) plane or (Power, Speed) plane, of existing (constructed) machines is a costly and time consuming task [19, 21, 22]. It should be noticed that it is mainly the (Torque, Speed) plane which is used in most technical and scientific publications to present EM. The cost and time are mainly dependent on the desired level of accuracy and the number of (Torque, Speed) or (Power, Speed) points (discretization of the search space) for which acquisitions are required.

This issue of time consumption is also present when the efficiency mapping is used for conception and design purposes. When used for conception and design, the efficiency mapping is often used to compare the performance of different machines whether qualitatively [conception (comparison of the performance of different machine types)] or quantitatively [design (comparison of the performance of different designs of a given machine type)].

In this contribution, the EM is defined as the maximum efficiency contour plots in (Torque, Speed) or (Power, Speed) planes [23, 24]. Figure 1.1 illustrates the problematic of efficiency mapping when used to assess the electrical machines performance experimentally (Fig. 1.1a) [2, 19], and when used for conception and design purposes (Fig. 1.1b) [1–18]. In both cases, the process allowing obtaining the EM mainly consists in the selection of operating conditions allowing maximizing

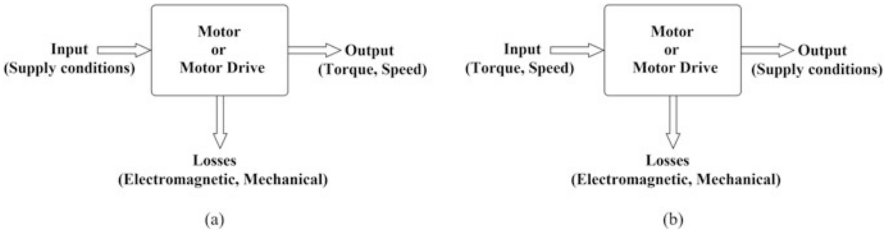

Fig. 1.1 Efficiency mapping [5]

efficiency for a set of (Torque, Speed) points. Two main parameters having an important impact on the time consumption issue can be identified:

1. the discretization of the search space [EM depends on many parameters, with some internal (supply conditions, for example) and some are external (environment temperature, for example)];
2. the machine modelling approach (for experimental EM determination, it is the constructed machine and the acquisition system).

The EM accuracy is clearly improved if the search space is finely meshed and the used models (or acquisition system in case of experimental establishment of the EM) are highly precise, but this come at the price of a workload, cost and time consumption which may prohibit such exercise [21].

Concerning the discretization of the search space issue, many researchers propose to reduce the search space and find adequate interpolation techniques [2, 11]. Neural networks seem to be privileged by some researchers as an interpolation tool [2, 11, 25]. The neural network can be seen as a replacement light model of the machine in case of an experimental establishment of the EM, or more precise models (often based on the finite element method) used for design purposes.

This brings the discussion to lighter models which can help reduce time consumption. This discussion is all the more relevant because the subject of this contribution is the use of EM for predesign purposes [16]. In different contributions, many researchers proposed modelling approaches to establish EM with reduced time [2, 11, 16, 18, 21, 22, 25–29].

Basically, as the finite element method (FEM) has been proven to be an accurate and precise modelling approach as compared to experimental measurements in different engineering domains, due to many advantageous features, it is often used in the design of engineering devices. One of the main reasons of its accuracy is the reduced number of simplifying assumptions, and its ability to consider important physical phenomenon operating in the studied devices. This is why many studies rely on FEM for the establishment of the EM [8, 11, 18, 22, 25, 26, 30]. Nevertheless, it is considered as time consuming when it comes to the optimization design of devices. Different researchers propose to use it (FEM) along other techniques [11, 22, 26], or to use lighter modelling approaches [4, 6, 7, 15–17, 31]. Nowadays, many software editors includes tools for efficiency maps estimation [21, 22, 32, 33], and companies specialized in measurements and acquisition solutions are proposing equipment to experimentally establish EM [19].

In this contribution, equivalent electrical circuits modelling approach is adopted [4, 6, 7, 15–17, 31]. Even if the different losses modelling can be considered as basic in this approach, its accuracy is acceptable at a predesign stage [16]. Furthermore, more accurate loss function [24] can be adopted along with the equivalent electrical circuits modelling approach. The adopted modelling approach is discussed in the following section.

1.3 Synchronous Machines Models

The efficiency maps estimation is based on the classical electrical circuits model in the Park referential frame (synchronous *d*–*q* reference frame) [6, 34, 35]. The model used in this study is not detailed because it has already been presented in [6, 16]. Its main characteristics are recalled. Figure 1.2a, b show equivalent circuits for armature windings, and Fig. 1.2c shows an equivalent circuit for the wound field excitation. For PM and synchronous reluctance machines, the wound field excitation circuit doesn't exist. Main symbols in these figures are defined as:

i_d, i_q	*d* and *q* axes components of armature current,
I_e	excitation current,
i_{fd}, i_{fq}	*d* and *q* axes components of iron loss current,
v_d, v_q	*d* and *q* axes components of terminal voltage,
V_e	excitation coils terminal voltage,
R_a	armature winding resistance per phase,

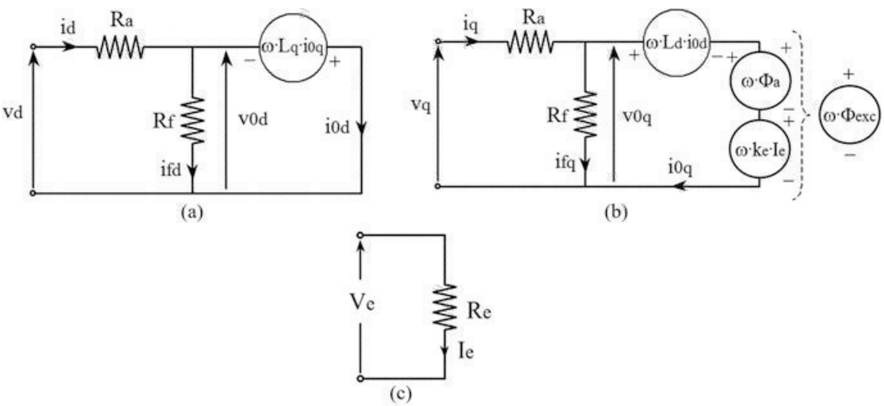

Fig. 1.2 Synchronous machines equivalent circuits model under motor mode operation. (**a**) *d* axis equivalent circuit. (**b**) *q* axis equivalent circuit. (**c**) Wound field excitation equivalent circuit

Table 1.1 Model adjustment for the different synchronous machines

Machine type	Parameters
PM synchronous machines	$k_e = 0$ H
Wound field synchronous machines	$\Phi_a = 0$ Wb
Hybrid excited synchronous machines	$k_e \neq 0$ H, $\Phi_a \neq 0$ Wb
Synchronous reluctance machines	$k_e = 0$ H, $\Phi_a = 0$ Wb

R_f iron loss resistance,
R_e excitation coils resistance,
Φ_a permanent magnet flux linkage,
Φ_{exc} total excitation flux linkage,
k_e "Armature/Excitation windings" mutual inductance,
L_d, L_q d and q axes components of synchronous inductance.

Table 1.1 describes the adjustment to operate in order to adapt the model to the different types of synchronous machines.

The approach presented in this contribution is intended to be used in the initial design steps of electrical drives based on synchronous machines. Its originality lies on the combination of the use of electric circuits modelling, and its versatility to allow the consideration of different synchronous machines types. This makes the proposed approach easily usable to rapidly assess the applicability of different synchronous machines types in variable speed applications. The versatility of the approach should be also appreciated by its ability to consider more precisely some physical phenomenon, as magnetic saturation, or more accurate iron loss models, but at the price of an increased computation time. The magnetic saturation can be considered through its effects on flux linkage and inductances. The consideration of PWM and space harmonics effects on the iron losses can be considered by a more accurate model of the resistance R_f. Besides, it should be highlighted that similar approach has been used for the study of efficiency maps of induction machines [31].

1.3.1 Per-Unit System

Per unit system model allows a better understanding of parameters effect on machines performance. It is also a powerful tool for electric machines drives classification [36–38]. For excited synchronous machines, i.e., pure wound field excited synchronous machines, PM synchronous machines and hybrid excited synchronous machines, base values of EMF and current are chosen as the rated values for the motor at rated speed (base speed Ω_b). For more details, readers are invited to consult references [6, 16], where variation ranges are provided. The previous per-unit system [6, 15, 16] is extend to the case of synchronous reluctance machines.

Synchronous reluctance machines being not excited, it is impossible to define normalized quantities in relation to the excitation flux. In the following Eq. (1.1),

Table 1.2 Normalised parameters variations intervals

Parameter	Variations interval
I_n (normalized current)	[0, 1]
V_n (normalized voltage)	[0, 1]
P_n (normalized power)	[0, 1]
Ω_{n} (normalized speed)	[0, +∞[
Γ_n (normalized torque)	[0, 1]
ρ (saliency ratio)	]1, +∞[
L_{dn} (normalized d axis inductance)	]0, +∞[
R_{an} (normalized armature resistance)	[0, 1[
R_{fn} (normalized iron loss resistance)	]0, +∞[

the normalized quantities and parameters are redefined for these machines:

$$V_n = \frac{V}{V_{\max}},\ L_{dn} = \frac{L_d \cdot I_{\max} \cdot \omega_b}{V_{\max}},\ R_{an} = \frac{R_a \cdot I_{\max}}{V_{\max}},\ R_{fn} = \frac{R_f \cdot I_{\max}}{V_{\max}}, \tag{1.1}$$

where, ω_b is the electric pulsation at the base speed.

It should be noticed that contrary to excited synchronous machines where the d axis is defined as the axis of maximum excitation flux, it is not possible to distinguish between the d and q axes for synchronous reluctance machines. The d axis is chosen in this contribution as the minimum inductance axis. Table 1.2 provides some variational ranges of the different normalized quantities and parameters in this new framework.

1.4 Efficiency Maps Computation

The efficiency map estimation discussed in this contribution is done for the optimal control allowing maximizing the efficiency, while respecting the current and voltage limits constraints.

1.4.1 Non-salient Poles Machines

The study discussed in this contribution is the continuity of the work presented in [6, 16]. In [6, 16], the efficiency maps estimation is detailed for non-salient synchronous machines (saliency ratio $\rho = L_q/L_d = 1$), which structurally excludes the synchronous reluctance machines.

Due to simplifications in the synchronous machines equations for $\rho = 1$, many mathematical developments required to determine the triple (i_d, i_q, I_e), or (I, ψ, k_f), allowing maximizing the efficiency, while respecting the current and voltage limits constraints, are done analytically [16]. I, ψ, and k_f are respectively the armature current amplitude, armature current/EMF (per phase) phase shifting, and the excitation coefficient ($= \Phi_{exc}/\Phi_{exc\,\max}$) [16].

The codes developed under MATLAB environment, allowing the estimation of the efficiency maps for these machines, are made available to the readers through the link given as reference [39]. They will be used to validate codes developed in the case of salient poles machines, the non-salient poles machines being considered as a particular case of salient poles ones.

1.4.2 Salient Poles Machines

The developments presented in this section are more general and applicable to all synchronous machines types: wound field, PM, hybrid excited and synchronous reluctance motors.

Due to more complicated equations, the analytical developments are limited, and most of the steps allowing the determination of the triple (I, ψ, k_f) maximizing the efficiency are done numerically. The previous case (non-salient pole machines) could be regarded as a particular case of these more general developments. Results from previous developments are exploited to assess the validity of these more general developments.

From Fig. 1.2, the armature voltage equations are expressed as

$$\begin{bmatrix} v_d \\ v_q \end{bmatrix} = R_a \cdot \begin{bmatrix} i_d \\ i_q \end{bmatrix} + \begin{bmatrix} v_{0d} \\ v_{0q} \end{bmatrix}, \tag{1.2}$$

$$\begin{bmatrix} v_{0d} \\ v_{0q} \end{bmatrix} = \begin{bmatrix} 0 & -\omega \cdot L_q \\ \omega \cdot L_d & 0 \end{bmatrix} \cdot \begin{bmatrix} i_{0d} \\ i_{0q} \end{bmatrix} + \omega \cdot \Phi_{exc} \cdot \begin{bmatrix} 0 \\ 1 \end{bmatrix}, \tag{1.3}$$

and torque equation is given by

$$\Gamma = p \cdot i_{0q} \cdot \left(\Phi_{exc} + \left(L_d - L_q\right) \cdot i_{0d}\right). \tag{1.4}$$

where, p is the number of pole pairs. Note that for synchronous reluctance machines $\Phi_{exc} = 0$ Wb.

The first step towards the determination of efficiency maps is the computation of $V_{n\,\max}$, the normalized value of armature windings terminals maximum voltage [16], for the excited synchronous machines, and L_{dn} for synchronous reluctance machines. This corresponds to the determination of the base speed Ω_b. The MATLAB scripts used in order to determine the value of $V_{n\,\max}$ is given in Table 1.3 for excited synchronous machines. For synchronous reluctance machines $V_{n\,\max} = 1$.

The determination of base speed allows defining remaining normalised quantities and parameters. Tables 1.4 and 1.5 summarize the definition of the normalized quantities from real ones for excited synchronous machines and synchronous

Table 1.3 Algorithm inside inner loop for a given (Ω_n, Γ_n, k_f) combination

```
Start
Values of L_dn, L_qn, R_an and R_fn should have been defined
I_n = [0: step_I : 1];
ψ = [−90 : step_ψ : 90];
For i = 1 : length(I_n)
    For j = 1 : length(ψ)
            i_dn (j) = −I_n (i) · sin(ψ(j));
            i_qn (j) = I_n (i) · cos(ψ(j));
            i_0dn (j) = f (i_dn (j), i_qn (j)); [see Eq. (1.6)]
            i_0qn (j) = g (i_dn (j), i_qn (j)); [see Eq. (1.6)]
            Γ (j) = h (i_0dn (j), i_0qn (j)); [see Eq. (1.5)]
    End
    [Y1(i), X1(i)] = max(Γ );
    Γ_1 (i) = Γ (X1(i));
    ψ_1(i) = ψ(X1(i));
End
[Y2, X2] = max(Γ_1);
I_n1 = I_n(X2);
ang_2 = ang_1(X2);
I_dn = − I_n1 · sin(ang_2 · π / 180);
I_qn = I_n1 · cos(ang_2 · π / 180);
I_0dn = f (I_dn, I_qn); [see Eq. (1.5)]
I_0qn = g (I_dn, I_qn); [see Eq. (1.5)]
V_nmaxd = (R_an · I_dn − L_qn · I_0qn);
V_nmaxq = (R_an · I_qn 1 + L_dn · I_0dn + 1);
V_nmax = sqrt(V_nmaxd ^2 + V_nmaxq ^2);
End
```

Table 1.4 Defining the normalized quantities from real ones for excited synchronous machines

Initial real data	p, ρ, L_d, R_s, R_f, $\Phi_{exc\,\max}$, $V_{\max}$, $I_{\max}$
Unknown real quantities	We have two unknowns: ψ_{Opt} (angle ψ maximizing the torque at the base speed) and Ω_b (base speed). We need two equations to determine them: $\begin{cases} \max(\Gamma_{em}) \\ V = V_{\max} \end{cases}$ (MPTA control law)
Known reduced values from initial real data	ρ, L_{dn}
Unknown reduced values	ψ_{Opt}, $V_{n\,\max}$, R_{sn}, R_{fn} Note that the normalized values, $V_{n\,\max}$, R_{sn}, and R_{fn} are all related to the base speed value Ω_b. They are known therefore if the base speed is known.

reluctance machines respectively. Normalized quantities and parameters will be used in all further developments.

Even if strong similarities exist within the efficiency mapping calculations for any synchronous machine, whether it is excited (permanent magnet, wound excitation and hybrid excited machines) or not (variable-reluctance synchronous machines), there are differences due to the use of different normalization systems [40].

Table 1.5 Defining the normalized quantities from real ones for synchronous reluctance machines

Initial real data	p, ρ, L_d, R_s, R_f, $V_{\max}$, $I_{\max}$
Unknown real quantities	We have two unknowns: ψ_{Opt} (angle ψ maximizing the torque for the base speed) and Ω_b (base speed). We need two equations to determine them: $\begin{cases} \max(\Gamma_{em}) \\ V = V_{\max} \end{cases}$ (MPTA control law)
Known reduced values from initial real data	ρ, R_{sn}, R_{fn}
Unknown reduced values	ψ_{Opt}, L_{dn}

Normalized torque and relations between (i_{0dn}, i_{0qn}) and (i_{dn}, i_{qn}) are given by

$$\Gamma_n = \frac{i_{0qn} \cdot \left(k_f + (1-\rho) \cdot L_{dn} \cdot i_{0dn}\right)}{V_{n\max}}. \tag{1.5}$$

$$\begin{bmatrix} i_{0dn} \\ i_{0qn} \end{bmatrix} = \frac{1}{\Delta} \cdot \begin{bmatrix} 1 & \frac{\Omega_n \cdot \rho \cdot L_{dn}}{R_{fn}} \\ \frac{-\Omega_n \cdot L_{dn}}{R_{fn}} & 1 \end{bmatrix} \cdot \begin{bmatrix} i_{dn} \\ i_{qn} - \frac{\Omega_n \cdot k_f}{R_{fn}} \end{bmatrix}, \tag{1.6}$$

with, $\Delta = \left(1 + \frac{\rho \cdot (\Omega_n \cdot L_{dn})^2}{R_{fn}^2}\right)$.

In order to avoid unnecessary redundancy with previous contributions [4, 16], the model and its normalized version hasn't been detailed. Readers interested in the used model and the use of normalized quantities can consult dedicated references [4, 16, 34–38].

For synchronous reluctance machines, the value of L_{dn} is determined by first computing the value of ψ_{Opt}. This value is determined by maximizing the torque, which is for synchronous reluctance machines given by

$$\Gamma_n = (1-\rho) \cdot L_{dn} \cdot i_{0qn} \cdot i_{0dn}. \tag{1.7}$$

The value of ψ_{Opt} is given by

$$\psi_{Opt} = \frac{\pi}{2} + \frac{1}{2} \cdot \text{Arccos}\left(\frac{\left(\frac{\Omega_n \cdot L_{dn}}{R_{fn}}\right) \cdot (\rho+1)}{\sqrt{\left(\left(\frac{\Omega_n \cdot L_{dn}}{R_{fn}}\right) \cdot (\rho+1)\right)^2 + \left(\rho \cdot \left(\frac{\Omega_n \cdot L_{dn}}{R_{fn}}\right)^2 - 1\right)^2}}\right) \tag{1.8}$$

The value of L_{dn} is then determined from the normalized value of maximum armature voltage given by

$$V_{n\,\max} = 1 = \sqrt{\left(R_{an} \cdot i_{dn} - \rho \cdot L_{dn} \cdot i_{0qn}\right)^2 + \left(R_{an} \cdot i_{qn} + L_{dn} \cdot i_{0dn}\right)^2}, \qquad (1.9)$$

which leads to the following equation:

$$\left[\begin{array}{l} 2 \cdot \left(R_{an}^2 - 1\right) \cdot \left(R_{fn}^2 + \rho \cdot L_{dn}^2\right)^2 + 4 \cdot R_{an} \cdot R_{fn} \cdot \rho \cdot L_{dn}^2 \cdot \left(R_{fn}^2 + \rho \cdot L_{dn}^2\right) \\ +2 \cdot R_{fn}^2 \cdot \rho^2 \cdot L_{dn}^4 + R_{fn}^4 \cdot L_{dn}^2 \cdot \left(1+\rho^2\right) \\ +(1-\rho) \cdot L_{dn} \cdot R_{fn}^2 \cdot \left(\frac{R_{fn}^3 \cdot L_{dn}^2 \cdot (\rho+1)^2 + 2 \cdot \left(R_{an} \cdot \left(R_{fn}^2 + \rho \cdot L_{dn}^2\right) + \rho \cdot R_{fn} \cdot L_{dn}^2\right) \cdot \left(\rho \cdot L_{dn}^2 - R_{fn}^2\right)}{\sqrt{\left(R_{fn} \cdot L_{dn} \cdot (\rho+1)\right)^2 + \left(\rho \cdot L_{dn}^2 - R_{fn}^2\right)^2}}\right) \end{array}\right] = 0.$$

Considering that the values of R_{an} and R_{fn} are known, solving previous equation allows obtaining the value of L_{dn}. This equation is solved numerically. The value of L_{dn}, solution of this equation, is searched near a value, corresponding to its value when the different losses are neglected, i.e., $R_{an} = 0$ and $R_{fn} \to +\infty$, which is given by [40]

$$L_{dn} = \sqrt{\frac{2}{\rho^2 + 1}}. \qquad (1.10)$$

From the normalized expression of the torque Eq. (1.5), it is possible to determine a second order polynomial of the normalized current amplitude (1.11).

$$A \cdot I_n^2 + B \cdot I_n + C = 0, \qquad (1.11)$$

with,

$$\begin{array}{l} A = \left[L_{dn} \cdot (1-\rho) \cdot \left(\frac{\Omega_n \cdot \rho \cdot L_{dn}}{R_{fn}} \cdot \cos\psi - \sin\psi\right) \cdot \left(\frac{\Omega_n \cdot L_{dn}}{R_{fn}} \cdot \sin\psi + \cos\psi\right)\right], \\ B = \left[\left(\frac{\Omega_n \cdot L_{dn}}{R_{fn}} \cdot \sin\psi + \cos\psi\right) \cdot (1 + \rho \cdot (\Delta - 1)) \cdot k_f - \left(\frac{\Omega_n \cdot k_f}{R_{fn}}\right) \cdot L_{dn} \cdot \right. \\ \left. (1-\rho) \cdot \left(\frac{\Omega_n \cdot \rho \cdot L_{dn}}{R_{fn}} \cdot \cos\psi - \sin\psi\right)\right], \\ C = \left[-\left(\frac{\Omega_n \cdot k_f^2}{R_{fn}}\right) \cdot (1 + \rho \cdot (\Delta - 1)) - \Gamma_n \cdot \Delta^2 \cdot V_{n\,\max}\right]. \end{array}$$

For a given (Ω_n, Γ_n, k_f, ψ) set, if Eq. (1.11) doesn't have a solution, the efficiency is set null $\eta = 0$. In case solutions exist, the current limit constraint ($I_n \leq 1$), and the voltage limit constraint ($V_n \leq V_{nmax}$), have to be respected both, otherwise the efficiency is set null $\eta = 0$.

In case Eq. (1.11) has two solutions and both allow respecting the current and voltage limits constraints, the one which is retained is the one allowing maximizing the efficiency.

For synchronous reluctance machines, the excitation coefficient is null, and Eq. (1.11) simplifies to

$$A \cdot I_n^2 + C = 0, \qquad (1.12)$$

with,

$$A = \left[L_{dn} \cdot (1-\rho) \cdot \left(\frac{\Omega_n \cdot \rho \cdot L_{dn}}{R_{fn}} \cdot \cos\psi - \sin\psi\right) \cdot \left(\frac{\Omega_n \cdot L_{dn}}{R_{fn}} \cdot \sin\psi + \cos\psi\right)\right],$$
$$C = \left[-\Gamma_n \cdot \Delta^2\right].$$

For a given (Ω_n, Γ_n, ψ) set, if Eq. (1.12) doesn't have a solution, the efficiency is set null $\eta = 0$. In case solutions exist, the current limit constraint ($I_n \leq 1$), and the voltage limit constraint ($V_n \leq 1$), have to be respected both, otherwise the efficiency is set null $\eta = 0$.

Figure 1.3 shows the algorithms used to calculate the efficiency maps for excited synchronous machines (Fig. 1.3a), and synchronous reluctance machines (Fig. 1.3b). The algorithm allows determining the (I_n, ψ, k_f) triple or the (I_n, ψ) couple maximizing the efficiency for each operating point for excited synchronous machines or synchronous reluctance machines, respectively.

For excited synchronous machines, the computer code developed to plot the efficiency mappings contains four loops, and three loops for the synchronous reluctance machines. In the code dedicated to excited machines, the additional loop as compared to synchronous reluctance machines concerns the excitation coefficient (Fig. 1.3a).

For the excited synchronous machines, the two external loops, which concern the torque and speed, or the two internal loops, which concern ψ and k_f, are both interchangeable. For synchronous reluctance machines, the external loops, which concern the torque and speed, are also interchangeable. There is only one internal loop, which concerns the phase shifting ψ. For excited synchronous machines, it should be noted that the internal loop concerning the excitation coefficient k_f can be replaced exactly by a loop for the normalized amplitude of the armature current I_n [40] (Fig. 1.4). Indeed, Eq. (1.11) can be easily rewritten, leading to an equation quadratic in the excitation coefficient k_f (1.13). Figure 1.4 shows the algorithm when the internal loop concerning the excitation coefficient k_f is replaced by a loop for the normalized amplitude of the armature current I_n.

The equation quadratic in the excitation coefficient k_f is given by

$$A \cdot k_f^2 + B \cdot k_f + C = 0, \tag{1.13}$$

with,

$$A = \left[-\left(\frac{\Omega_n}{R_{fn}}\right) \cdot (1 + \rho \cdot (\Delta - 1))\right],\ B = \left[\left(\frac{\Omega_n \cdot L_{dn}}{R_{fn}} \cdot \sin\psi + \cos\psi\right) \cdot (1 + \rho \cdot (\Delta - 1)) \cdot I_n\right],$$
$$C = \left[\begin{array}{l} L_{dn} \cdot (1-\rho) \cdot I_n^2 \cdot \left(\frac{\Omega_n \cdot \rho \cdot L_{dn}}{R_{fn}} \cdot \cos\psi - \sin\psi\right) \cdot \left(\frac{\Omega_n \cdot L_{dn}}{R_{fn}} \cdot \sin\psi + \cos\psi\right) \\ -\left(\frac{\Omega_n \cdot k_f}{R_{fn}}\right) \cdot L_{dn} \cdot (1-\rho) \cdot \left(\frac{\Omega_n \cdot \rho \cdot L_{dn}}{R_{fn}} \cdot \cos\psi - \sin\psi\right) \cdot I_n - \Gamma_n \cdot \Delta^2 \cdot V_{n\max} \end{array}\right].$$

In the case of the algorithm illustrated by Fig. 1.4, it is not necessary to verify that the armature current amplitude limit is respected, since this is explicitly imposed by the variation range of the normalized armature current amplitude. Nevertheless, it

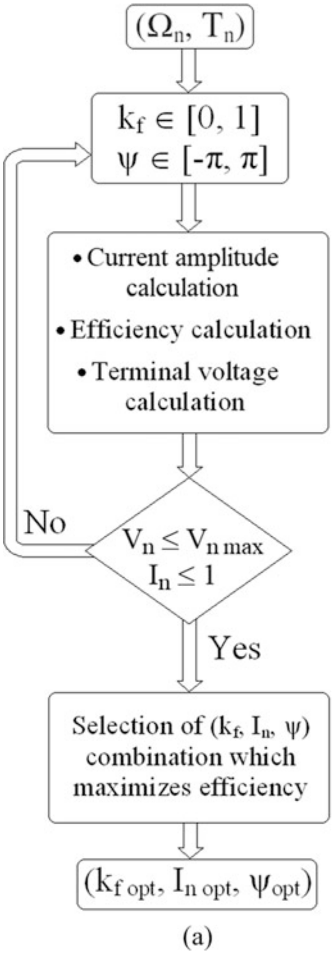

Fig. 1.3 Efficiency mapping computation algorithm. (**a**) Excited synchronous machines. (**b**) Synchronous reluctance machines

should be verified that voltage limit is respected, and that the excitation coefficient k_f is positive, and lower or equal to 1.

The code developed under MATLAB environment, and based on the previous algorithm, is made available to the readers through the link given as reference [41].

1.5 Tool Validation

The following step in this work is the validation of the algorithm and the subsequent developed codes [41]. The efficiency maps obtained from codes developed earlier, for non-salient synchronous machines [39], are compared to the ones issued from

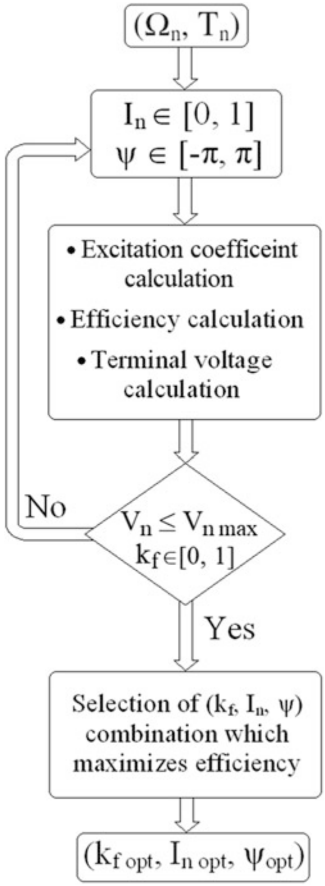

Fig. 1.4 Efficiency mapping computation algorithm for excited synchronous machines when the loop on k_f is replaced by a loop on I_n

the new codes [41]. The codes developed for non-salient synchronous machines have been used and assessed many times [4, 6, 16, 17].

Figure 1.5a, b compare efficiency maps for a non-salient hybrid excited synchronous machine with: $L_{dn} = 0.5$; $\rho = 1$; $R_{an} = 0.1$; $R_{fn} = 20$; $k_{en} = 1$; $R_{en} = 1$; $\beta = 27$; and $\alpha = 1$. β is the power ratings ratio between converters supplying the armature and excitation windings, respectively [16]. Hybridization ratio α, which is specific to HESM, is the ratio between the permanent magnet flux and the maximum excitation flux ($= \Phi_a/\Phi_{exc\,\max}$) [16]. These parameters have been derived from an existing prototype [6] [42]. As can be seen very good agreement is obtained between results issued from both codes.

Same comparison has been conducted for a wound field synchronous machine (Fig. 1.6) and a PM synchronous machine (Fig. 1.7). Both machines share following parameters: $L_{dn} = 0.5$; $\rho = 1$; $R_{an} = 0.1$; $R_{fn} = 20$. For the wound field synchronous machine the additional parameters are: $k_{en} = 1$; $R_{\mathrm{en}} = 1$; $\beta = 27$; and $\alpha = 0$. As can be seen very good agreement is again obtained for both machines.

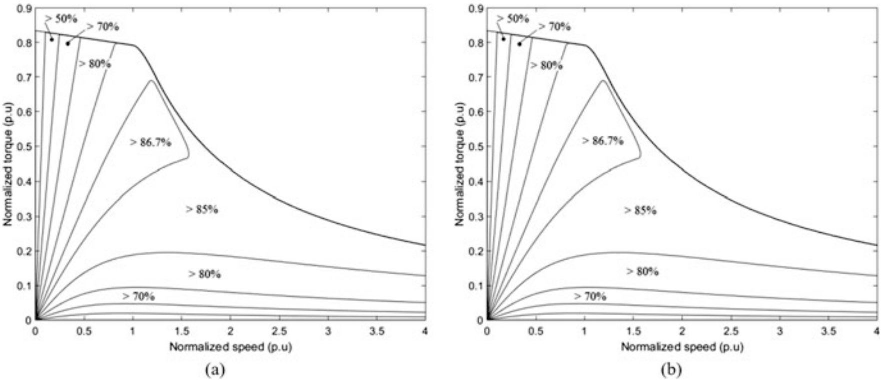

Fig. 1.5 Efficiency maps comparison (Hybrid excited machine). (**a**) Initial code. (**b**) New code

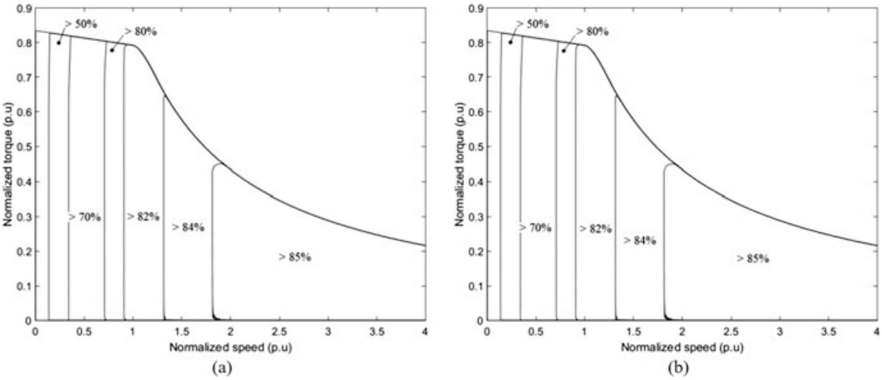

Fig. 1.6 Efficiency maps comparison (Wound field machine). (**a**) Initial code. (**b**) New code

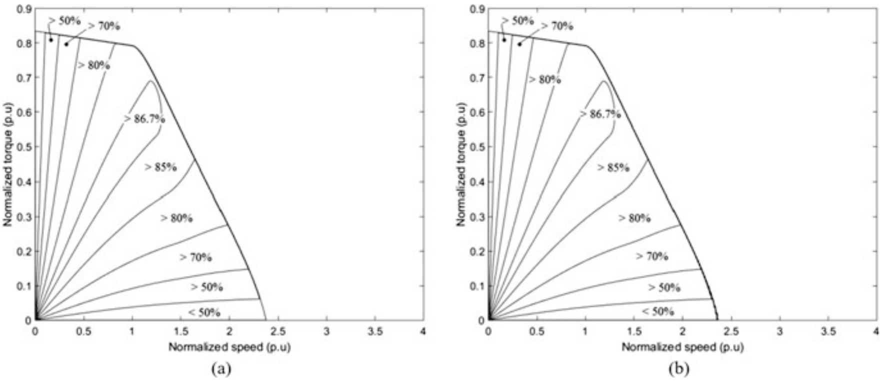

Fig. 1.7 Efficiency maps comparison (PM machine). (**a**) Initial code. (**b**) New code

It can be fairly concluded that the proposed algorithm and developed codes are trustable enough to be further used for analysis and design purposes.

In the following Sect. 1.6, the new codes are used to analyse the effects of saliency on the performance of PM synchronous machines and synchronous reluctance machines.

1.6 Tool Exploitation

In this section, the developed codes are used to perform preliminary analyses on the effect of saliency ratio on efficiency maps of PM synchronous machines and synchronous reluctance machines. The goal is not to perform a thorough analysis but rather to highlight the capabilities of developed tools.

1.6.1 PM Synchronous Machines

The developed codes are first used to study the effects of saliency ratio on the performance of PM synchronous machines. These machines share following parameters: $L_{dn} = 0.5$; $R_{an} = 0.1$; $R_{fn} = 20$. The saliency ratio is varied: $\rho = 0.5$, 1, 1.5, and 2. Figure 1.8 shows the efficiency maps for $\rho = 0.5$, 1.5, and 2. As compared to non-salient machines, presence of saliency allows increasing the torque.

The maximum torque is slightly increased. The maximum efficiency doesn't seem affected (Table 1.6). Table 1.6 gives maximum efficiency for the different machines.

The higher efficiency zones get wider as the saliency ratio increases as can be noticed from Figs. 1.7 and 1.8. The operating zone is also enlarged. While in Fig. 1.7 ($\rho = 1$) the maximum normalized speed is lower than 2.5, it is clearly higher than 2.5, for $\rho = 2$ (Fig. 1.8c). The saliency ratio increase seems to have a more important impact on the increase of the maximum operating speed, as compared to its impact on the increase of the maximum operating torque.

As compared to non-salient synchronous machines ($\rho = 1$), the increase of saliency ratio ($\rho > 1$) has a more important impact on the widening of operating area, as can have its reduction ($\rho < 1$). This result is coherent with results obtained in the study conducted in [15].

1.6.2 Synchronous Reluctance Machines

The codes are also exploited to study the effect of saliency ratio on the performance of synchronous reluctance machines. These machines share following parameters: